Michigan State University

National Superconducting Cyclotron Laboratory

FRAGMENTS IN GAUSSIAN WAVE-PACKET DYNAMICS WITH AND WITHOUT CORRELATIONS

DIETER KIDERLEN and PAWEL DANIELEWICZ

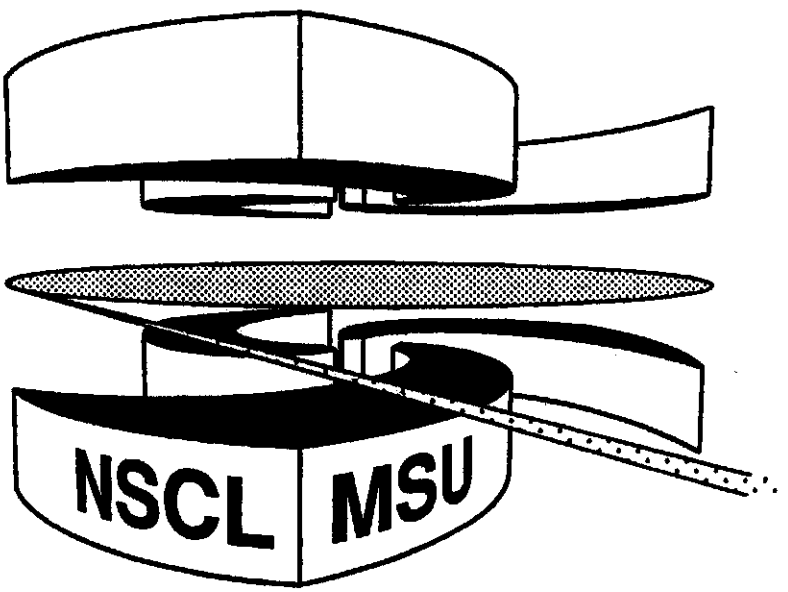

MSUCL-1047

NOVEMBER 1996

MSUCL-1047

Fragments in Gaussian Wave-Packet Dynamics with and without Correlations

Dieter Kiderlen* and Paweł Danielewicz†

National Superconducting Cyclotron Laboratory and

Department of Physics and Astronomy, Michigan State University,

East Lansing, Michigan 48824, USA

(November 13, 1996)

Abstract

Generalization of Gaussian trial wave functions in quantum molecular dynamics models is introduced, which allows for long-range correlations characteristic for composite nuclear fragments. We demonstrate a significant improvement in the description of light fragments with correlations. Utilizing either type of Gaussian wave functions, with or without correlations, however, we find that we cannot describe fragment formation in a dynamic situation. Composite fragments are only produced in simulations if they are present as clusters in the substructure of original nuclei. The difficulty is traced to the delocalization of wave functions during emission. Composite fragments are produced abundantly in the Gaussian molecular dynamics in the limit $\hbar \to 0$.

PACS numbers: 24.10.-i, 25.70.-s, 25.70.Pq

keywords: wave-packet dynamics, fragment production, correlations, FMD

*e-mail: kiderlen@nscl.msu.edu

†e-mail: danielewicz@nscl.msu.edu

I. INTRODUCTION

The theoretical description of heavy-ion collisions at intermediate beam energies, 10 MeV $\lesssim E/A \lesssim$ 150 MeV, is still in an unsatisfactory state. Different factors contribute to that situation. Thus, for one, the nucleon excitation energies are low and in that comparable to nucleon localization energies, indicating a likely importance of the quantal effects. With the change in the beam energy in the discussed range, the dynamics changes from that dominated by the mean field to that dominated by collisions (as evidenced in the appearance of the flow balance-energy). As excitation energies grow, they begin to exceed the average binding energies per nucleon and, within the mentioned range of E/A, a massive production of intermediate-mass fragments (IMF) takes place [1]. The production, in terms of IMF multiplicity or total mass that IMF carry, maximizes at $E/A \sim 75$ MeV. The description of the intermediate and light fragment production is beyond the capability of common single-particle models of collisions [2]. The single-particle models with fluctuating forces [3,4] can describe fragment production, but miss the shell effects and the discreteness of the mass and charge numbers. The involved limitation is recognized once one realizes that, in the very central Au + Au collisions at 100 MeV/nucleon, the probability for a proton to come out from the reaction as a constituent of an α particle is close [5] to 50%. Within the Boltzmann-Langevin model with the fluctuating forces [3,4], the α particle plays no distinguished role. Statistical models [6,7] account for the shell effects, but miss the reaction dynamics. The importance of the dynamics is seen, in particular, in the fact that the collective outward flow energy in the reactions is comparable to the thermal energy.

Given the above situation, the quantum molecular model proposed in recent years for the reactions [8] was met with quite some expectations. In this model, the quantal wave function for a reacting system is represented as a product of Gaussian wave-packets for individual nucleons. The packets have dynamic centers, phases, and widths. The parameters obey equations of motion following from a variational principle. The model [8] accounts for shell effects and has been shown to describe the evaporation of individual nucleons

from excited nuclei [9]. As nucleons leave a nucleus, their wave-packets become completely delocalized. The packets are used in this model in favor of the Hartree-Fock wave-functions, because with the packets one expects to describe fluctuations. Note that initialization of the classical Vlasov equation with a set of δ-functions leads to the same results as the exact equations of motion. The set of wave-packets is the closest approximation to the set of δ-functions that one can get quantally. Other molecular models in use might be considered amended or simplified versions of [8]. Both in the model [8] (termed FMD) and in [10] (termed AMD), the overall wave function is antisymmetrized. However, in [10] the dynamics of the wave-packet width is suppressed. In [11] (EQMD) the width is dynamic, but the effects of antisymmetrization are accounted for only approximately, using a Pauli pseudopotential. In [12] and [13] (QMD) neither the widths are dynamic nor the antisymmetrization is carried out explicitly. These models are the most classical within the class. In the models AMD, EQMD, and QMD, collisions between wave packets take place, on top of the wave-packet dynamics obtained or attributable to the variational principle for wave functions.

Within the molecular models, fragment production has been studied, in quite some detail, in the most classical of the class, the QMD model [14,15]. Within the FMD model, the fragment emission has been observed in the calculations of reactions involving light nuclei [9]. In the FMD model a specific problem arises concerning the emission of fragments. Inside a fragment, the constituent nucleons are localized in the relative separations. When the wave function is a product of single-particle wave functions, this implies a localization of the fragment center of mass. While low-energy nucleons escaping from a nucleus become delocalized, getting rid of the kinetic energy associated with their localization [9], this cannot be the case for the fragments. The c.m. localization energies e.g. in the range of $A = (2$–$4)$ nuclei, are within $\Delta E \sim (10 - 30)$ MeV and, given that the temperatures in excited nuclei in reactions could be as low as (5–10) MeV, they could result in significant thermal penalty-factors for emission, $e^{-\Delta E/T}$.

Generally, within FMD and EQMD the kinetic energy of the localization of the center of mass is not conserved and may be transformed into the internal energy, in a translationally

invariant situation. While this need not be a problem for large fragments with a small localization energy compared to the fragment total energy, for light fragments it can mean that their excitation energies cannot be determined.

In this paper, we investigate fragment production within a model of the FMD type. Given the problems associated with the localization, mentioned above, we consider the wave functions, of a Gaussian form, that are products of wave functions for individual nucleons and also such that allow for the correlations between nucleons within fragments, with a decoupling of the fragment center of mass motion. At present, effects of antisymmetrization are accounted for approximately only using a Pauli potential.

The outline of the paper is as follows. Section II describes the trial wave functions for the Schwinger variational principle. The equations of motion following from that principle are discussed in Sec. III. Section IV discusses a choice of the hamiltonian which permits an analytic calculation of the expectation values in the equations. Our results on fragment dynamics and production are reported in Sec. V and the conclusions are given in Sec. VI.

II. TRIAL WAVE FUNCTION

The trial wave-function for the Schwinger variational principle is taken in the form

$$\langle \boldsymbol{x}_1, \ldots, \boldsymbol{x}_N | \Psi \rangle = \mathcal{N} \exp\Big(\phi(\boldsymbol{x}_1, \ldots, \boldsymbol{x}_N)\Big)\, \chi\,, \tag{1}$$

where χ is a normalized spin-isospin wave function. The argument in the unnormalized exponential wave function is

$$\phi(\boldsymbol{x}_1, \ldots, \boldsymbol{x}_N) = -A_{ij}\,(\boldsymbol{x}_i - \boldsymbol{r}_i)\cdot(\boldsymbol{x}_j - \boldsymbol{r}_j) + i\,\boldsymbol{p}_i\,\boldsymbol{x}_i. \tag{2}$$

Here, $\boldsymbol{x}_i$ denotes the position vector of particle i. The repeated particle indices indicate summation. In absence of antisymmetrization, from (1) and (2) one finds that the normalization constant is equal to $\mathcal{N} = (\det(2\,\mathrm{Re}\,A)/\pi^N)^{3/4}$, where N is the particle number.

The parameters of the spatial wave function, which depend on time, include the elements of the complex symmetric $3N \times 3N$ matrix A with a positive definite real part, and further

the components of the $2N$ real vectors $\{\boldsymbol{r}_i\}$ and $\{\boldsymbol{p}_i\}$. Below, we shall use q_ν to indicate any member of a set of the dynamic parameters. A convenient mapping of the set follows using $q_{i(i-1)/2+j} = \mathrm{Re}\, A_{ij}$ and $q_{N(N+1)/2+i(i-1)/2+j} = \mathrm{Im}\, A_{ij}$, where in the both equations $j \leq i$, and further using $q_{N(N+1)+3(i-1)+a} = (\boldsymbol{r}_i)_a$ and $q_{N(N+4)+3(i-1)+a} = (\boldsymbol{p}_i)_a$. The time-dependent parameters relate to different expectation values with

$$\langle \boldsymbol{x}_i \rangle = \boldsymbol{r}_i\,, \qquad\qquad \langle -i\,\nabla_i \rangle = \boldsymbol{p}_i\,, \tag{3}$$

$$\langle (\boldsymbol{x}_i)_a\,(\boldsymbol{x}_j)_b \rangle = (\boldsymbol{r}_i)_a\,(\boldsymbol{r}_j)_b + \frac{\delta_{ab}}{4}\,(\mathrm{Re}A)^{-1}_{ij} \tag{4}$$

and

$$\langle i(\nabla_i)_a\, i(\nabla_j)_b \rangle = (\boldsymbol{p}_i)_a\,(\boldsymbol{p}_j)_b + \delta_{ab}\,(A^*\,(\mathrm{Re}\,A)^{-1}\,A)_{ij}\,, \tag{5}$$

where a and b are indices for carthesian coordinates. Given (3)–(5), the parameters $\boldsymbol{r}_i$ and $\boldsymbol{p}_i$ are referred to, further, as the centroid and momentum of a particle i, respectively, and A is referred to as the width matrix.

The form (1) includes the special case of the width diagonal in particle indices, $A_{ij} = \delta_{ij}\,A_i$. The wave function in that case reduces to a product of single-nucleon wave functions such as utilized in the FMD or EQMD calculations. To illustrate the advantage that (1) with (2) offers, let us consider a deuteron. The parametrization allows for the wave function of the form

$$\langle \boldsymbol{x}_1, \boldsymbol{x}_N | \Psi \rangle = \mathcal{N} \exp\Big(- A_{cm}(\boldsymbol{x}_1 + \boldsymbol{x}_2)^2/4 - A_{rel}(\boldsymbol{x}_1 - \boldsymbol{x}_2)^2 \Big)\,\chi\,, \tag{6}$$

where $A_{cm} = 2(A_{11} + A_{12})$, $A_{rel} = (A_{11} - A_{12})/2$, and $A_{11} = A_{22}$. The magnitude of A_{rel} can be adjusted to reproduce the r.m.s. radius of the deuteron and A_{cm} in the above may take on arbitrarily low values corresponding to a delocalized deuteron, as expected in the emission in reactions. FMD and EQMD parametrizations more standard than ours, with vanishing off-diagonal terms in A, on the other hand, permit only strongly localized deuterons, as $A_{cm} = 4A_{rel}$ for $A_{12} = 0$.

III. EQUATIONS OF MOTION

The wave function (1) depends on time only indirectly through the parameters q_μ. In this section, we shall obtain equations of motion (eom) that govern the behavior of these parameters.

On writing the time-dependent variational principle in the form $\delta \int_{t_1}^{t_2} \mathcal{L}(\dot{q}_\mu, q_\mu) dt = 0$, the eom for q_μ follow (formally) as Lagrange-Euler equations, $\frac{d}{dt}\frac{\partial \mathcal{L}}{\partial \dot{q}_\mu} - \frac{\partial \mathcal{L}}{\partial q_\mu} = 0$. Using $\mathcal{L} = \langle \Psi | i\hbar \frac{d}{dt} - H | \Psi \rangle$ for the Lagrange function, one obtains, see [9],

$$\mathcal{A}_{\nu\mu}\, \dot{q}_\mu = -\frac{\partial}{\partial q_\nu} \langle H \rangle \,, \tag{7}$$

where the matrix $\mathcal{A}$, multiplying the time derivatives, is skew symmetric. This matrix is related to the overlap of the derivatives of the wave function with respect to the parameters:

$$\mathcal{A}_{\nu\mu} = 2\,\mathrm{Im} \left\langle \frac{\partial}{\partial q_\nu} \Psi \middle| \frac{\partial}{\partial q_\mu} \Psi \right\rangle . \tag{8}$$

Given the wave function of the form (1), one finds for $\mathcal{A}$

$$\mathcal{A}_{\nu\mu} = 2\,\mathrm{Im} \left(\left[\frac{\partial \phi^*}{\partial q_\nu} \left(\frac{\partial \phi}{\partial q_\mu} - \left[\frac{\partial \phi}{\partial q_\mu} \right] \mathcal{N}^2 \right) \right] \mathcal{N}^2 + \left\{ \frac{\partial \chi}{\partial q_\nu} \middle| (1 - |\chi\}\{\chi|) \middle| \frac{\partial \chi}{\partial q_\mu} \right\} \right) , \tag{9}$$

where the square brackets stand for $[O] = \int \Pi_{l=1}^{N} d\boldsymbol{x}_l \exp(\phi^*) O \exp(\phi)$. From (9), one can see that $\mathcal{A}$ does not couple parameters describing spin-isospin degrees, with those in the spatial wave function. For an interaction diagonal in spin and isospin, considered below, this implies that the spin-isospin wave-function does not depend on time. Correspondingly, the spin-isospin wave functions will be largely disregarded in the further discussion.

The explicit expression for $\mathcal{A}$, obtained using (2), is

$$\mathcal{A}_{\nu\mu} = \frac{3}{4} (\mathrm{Re}\, A)^{-1}_{in} (\mathrm{Re}\, A)^{-1}_{jm} \frac{\partial\, \mathrm{Re}\, A_{ij}}{\partial q_\nu} \frac{\partial\, \mathrm{Im}\, A_{nm}}{\partial q_\mu} + \frac{\partial \boldsymbol{r}_i}{\partial q_\nu} \frac{\partial \boldsymbol{p}_i}{\partial q_\mu} - (\nu \leftrightarrow \mu) . \tag{10}$$

Since A is independent of $\boldsymbol{r}_i$ and $\boldsymbol{p}_i$, the eom for particle centroids and momenta take on the form of the Hamilton's equations with the expectation value of the Hamilton operator in these equations playing the role of a classical Hamiltonian. As far as the width is concerned, for a practical solution of the eom, it is necessary to invert the $\mathcal{A}$-matrix. When represented

in the space of the real and imaginary elements of A, the matrix $\mathcal{A}$ acquires a 2×2 block structure with the blocks on the diagonal vanishing and those off-diagonal (coupling the real and imaginary parts of A) given by $\pm\mathcal{B}$. Fortunately, the quadratic matrix $\mathcal{B}$, of a dimension $N(N+1)/2$, can be easily inverted analytically with the result

$$\mathcal{B}^{-1}_{\frac{n(n-1)}{2}+m,\frac{i(i-1)}{2}+j} = \frac{2}{3}\left(\mathrm{Re}\, A_{ni}\,\mathrm{Re}\, A_{mj} + \mathrm{Re}\, A_{nj}\,\mathrm{Re}\, A_{mi}\right), \tag{11}$$

where $1 \le m \le n \le N$, $1 \le j \le i \le N$. The equations of motion for the parameters – centroids, momenta, and matrix elements of A – take then on the form

$$\dot{\boldsymbol{r}}_i = \frac{\partial\langle H\rangle}{\partial \boldsymbol{p}_i}, \qquad \dot{\boldsymbol{p}}_i = -\frac{\partial\langle H\rangle}{\partial \boldsymbol{r}_i}, \tag{12}$$

$$\frac{d}{dt}\,\mathrm{Re}\, A_{ij} = \sum_{m\le n} \mathcal{B}^{-1}_{\frac{i(i-1)}{2}+j,\frac{n(n-1)}{2}+m}\,\frac{\partial\langle H\rangle}{\partial\,\mathrm{Im}\, A_{nm}}, \qquad \frac{d}{dt}\,\mathrm{Im}\, A = -\mathcal{B}^{-1}\,\frac{\partial\langle H\rangle}{\partial\,\mathrm{Re}\, A}. \tag{13}$$

The indices in the second equation in (13) should be handled in the same manner as in the first of the equations where they are written out explicitly. In evaluating the derivatives in (13), the elements $\mathrm{Re}\, A_{nm}$ and $\mathrm{Re}\, A_{mn}$, and $\mathrm{Im}\, A_{nm}$ and $\mathrm{Im}\, A_{mn}$, respectively, should be treated as identical.

Given (11), the contributions from the kinetic energy to the eom (13) for the width matrix may be simplified into

$$\mathcal{B}^{-1}\,\frac{\partial\langle T\rangle}{\partial\,\mathrm{Im}\, A} = \frac{2\hbar}{m}\,\mathrm{Im}\, A^2, \qquad \mathcal{B}^{-1}\,\frac{\partial\langle T\rangle}{\partial\,\mathrm{Re}\, A} = \frac{2\hbar}{m}\,\mathrm{Re}\, A^2. \tag{14}$$

For the free particles, eom may be then represented as $\dot{A} = -2i\hbar A^2/m$, with the solution $A(t) = A_0\,(1 + 2i\hbar(t-t_0)A_0/m)^{-1}$. This means that, for free particles, a width matrix diagonal initially in certain directions in the N-particle space will stay diagonal in these directions. Contributions to the kinetic energy associated with different directions, proportional to $|A(t)|^2/\mathrm{Re}\, A(t) = |A_0|^2/\mathrm{Re}\, A_0$, stay constant as a function of time. For interacting particles, clearly, interaction terms appear on the r.h.s. of the eom for the width. These terms can, generally, cause violations of the conservation law for the c.m. kinetic energy, when the width matrix is constrained to the diagonal form.

IV. HAMILTONIAN

The eom (12) and (13) express the time derivatives of the parameters q_μ in the wave function as the linear combinations of the derivatives of the expectation value of the Hamiltonian, with respect to q_μ. We shall now calculate the Hamiltonian expectation value in terms of the parameters.

The expectation value of the kinetic energy, $\langle T\rangle = -\frac{\hbar^2}{2m}\sum_i\langle\nabla_i^2\rangle$, is directly obtained from (5). To make the calculation of the expectation value of the potential analytic, we choose the internucleon potential of such a form as in [9],

$$V = \sum_k u_k \sum_{i<j}\Big(w_k + (1-w_k)P_{ij}^M\Big)\exp\Big(-\lambda_k^{-2}\,(\boldsymbol{x}_i-\boldsymbol{x}_j)^2\Big)\,, \tag{15}$$

where P_{ij}^M is the Majorana operator exchanging spatial coordinates of the particles i and j. The sum over k extends over the repulsive and attractive contributions to the potential. The values for u_k, λ_k and w_k are listed in [9]. With (15), we exclude the Coulomb potential as in [9], but then we only consider the light to medium nuclei. The expectation value of the potential (15) with respect to the wave function (1) is then

$$\langle V\rangle = \sum_k u_k \sum_{i<j}\mathcal{N}^2\Big[\exp\left(-\lambda_k^{-2}(\boldsymbol{x}_i-\boldsymbol{x}_j)^2\right)\Big(w_k+(1-w_k)P_{ij}^M\Big)\Big] \tag{16}$$

where the meaning of the square brackets is such as below Eq. (9). On defining the matrices Λ^{ij} and A_P by the relations, respectively, $\Lambda^{ij}_{nm}\boldsymbol{r}_n\cdot\boldsymbol{r}_m = (\boldsymbol{r}_i-\boldsymbol{r}_j)^2$ and $A^P_{nm} = A_{P(n)\,P(m)}$, where P exchanges indices i and j, we obtain

$$\Big[\exp(-\lambda_k^{-2}\,(\boldsymbol{x}_i-\boldsymbol{x}_j)^2)O\Big] = \frac{\pi^{3N/2}}{\Big(\det(A+A^{O*}+\lambda_k^{-2}\,\Lambda^{ij})\Big)^{3/2}}\,\exp(\varphi_O^{ij,k})\,. \tag{17}$$

The argument of the exponential on the r.h.s. of (17) for the two cases of the operator O is

$$\varphi_{O=1}^{ij,k} = -\frac{(\boldsymbol{r}_i-\boldsymbol{r}_j)^2}{2\lambda_k^2}\left(\Lambda^{ij}\,(2\,\mathrm{Re}A+\lambda_k^{-2}\,\Lambda^{ij})^{-1}\,\mathrm{Re}A\right)_{ii}\,, \tag{18}$$

and

$$\varphi_{O=P}^{ij,k} = -\frac{(A+A^{P*}+\lambda_k^{-2}\,\Lambda^{ij})^{-1}_{nm}}{4}\,\boldsymbol{q}_n^P\,\boldsymbol{q}_m^P - \frac{(A+A^{P*})_{nm}}{4}\,\boldsymbol{s}_n^P\,\boldsymbol{s}_m^P\,, \tag{19}$$

with $\boldsymbol{s}_n^P = \boldsymbol{r}_n - \boldsymbol{r}_{P(n)}$ and $\boldsymbol{q}_n^P = \boldsymbol{p}_n - \boldsymbol{p}_{P(n)} - i(A - A^{P*})_{nm}\boldsymbol{s}_m^P$.

At first glance, the calculation of $\langle V \rangle$ for non-diagonal width-matrix A scales with the number N of particles as N^5; for each of $N(N-1)/2$ particle pairs, one has to invert a $N \times N$ symmetric matrix. Fortunately, for each of the particle pairs the matrix that needs to be inverted differs from the matrix $2\,\mathrm{Re}\,A$ only in $4N - 6$ elements. Thus, for each of these pairs one can use information from inverting the matrix $\mathrm{Re}\,A$, and the calculation of $\langle V \rangle$ scales then only with the particle number as N^4.

Generally, one would want the trial wave function to be antisymmetrized. However, the width matrix A nondiagonal in particle indices introduces such a number of parameters, that the antisymmetrization ceases to be feasible for the particle number larger than ~ 16. Thus, we resort to the Pauli potential to simulate the effects of antisymmetrization. The Pauli potential acts only between particles with the same spin and isospin, and it is chosen proportional to the Majorana operator, $V_{Pauli} = u_3 P_{ij}^M$. The latter is motivated by the fact that the expectation value of P^M for the product wave function is proportional to the square of the scalar product of single-particle wave functions, $\langle P_{ij}^M \rangle = |\langle \psi_i | \psi_j \rangle|^2$, where $\psi_{i,j}$ are the single-particle wave functions of the two particles. When one wave function approaches another, the system reacts with a repulsive force. The Pauli potential is added as the third component to (15) ($w_3 = 0$, $\lambda_3^{-1} = 0$), and the value of u_3 is adjusted to best fit the properties of ground-state nuclei. Unfortunately, such u_3 depends quite significantly on the mass. Using parameter set $B1$ from [9] (originally from [16]) in (15), we obtain e.g. optimal $u_3 = 70$ MeV for $A = 12$ and $u_3 = 200$ MeV for $A = 80$. (This would have been likely partly alleviated if we included the Coulomb potential.)

As an example, in the obtained ground state of ^{12}C three four-fold degenerate centroids position themselves at the corners of an equilateral triangle in configuration space. The average associated particle momenta are zero. For the diagonal width matrix and the $B1$ interaction, the minimum internal energy (defined as the difference between the total energy and the energy of the center of mass motion) of $E_{int} = -87.1$ MeV is obtained for $\mathrm{Re}\,A_{ii} = 0.33$ fm^{-2} which gives $R_{rms} = 2.32$ fm. The obtained ^{12}C nucleus is stable against

break up into three α particles which have a ground state energy of $E_{int} = -28.1$ MeV. (Note that the ^{12}C energy does not contain the Coulomb energy estimated at $E_C = 11.4$ MeV using the formula (61) in [9]; the value of R_{rms} includes the spatial extent of a proton [9].) For the width matrix with off-diagonal elements, a lower minimum of $E_{int} = -95.4$ MeV is obtained for Re $A_{ii} = 0.30$ fm^{-2}, and Re $A_{ij} = -0.038$ fm^{-2}, if j is within the same cluster as i or has the same spin and isospin directions as i, and Re $A_{ij} = 0$, otherwise. There is a freedom, in the latter case, of adding a constant to all elements of A that only changes constraints on the c.m. motion.

For even-even nuclei of mass larger than carbon, our Pauli potential favors differences in average single-particle momenta over differences in centroids in the ground state. The centroids for these nuclei become identical while the momenta get distributed in momentum space in the groups of four. For example, in the ground state of ^{16}O the momenta are placed at the corners of a tetrahedron in momentum space.

V. SOLUTION OF THE EQUATIONS OF MOTION

We first discuss differences in the dynamics of isolated light fragments, for correlated and uncorrelated trial functions. We then investigate fragment production within the present dynamic description, when a compressed and excited nuclear system expands and when nuclei collide at low energies. Some of our results are quite unexpected.

Since the differences in the dynamics for correlated and uncorrelated trial functions are expected to be the largest for the lightest of fragments, we investigate the dynamics of an isolated deuteron and of an isolated α particle, illustrated in Figs. 1 and 2, respectively. As the deuteron is unbound for all the interactions listed in [9], we use the Volkov 1 (V1) [17] with $u_a = -104.5$ MeV in the deuteron case. Fig. 1a displays the evolution of total E_{tot}, kinetic E_{kin}, potential E_{pot}, and total internal E_{int} energies, for a deuteron initialized in the state of the lowest internal energy. Either the dynamics for a correlated (labeled c) or uncorrelated (labeled u) trial-function is followed. In the case of the correlated dynamics,

both the total and the internal energies remain constant as a function of time. However, in the case of the uncorrelated dynamics, the internal energy increases, at a cost of the center-of-mass energy. At $t \sim 12$ fm/c the deuteron becomes, in effect, unbound and it remains so thereafter. The different evolution is associated with the behavior of matrix elements, as illustrated in Fig. 1b. In the absence of correlations between particles, i.e. $A_{12} = 0$ in Eq. (6), the delocalization of the deuteron center of mass couples to the delocalization of the internal state. In particular, a reduction in Re A_{cm} requires a reduction in Re A_1 and this implies a reduction in Re A_{rel}. By contrast, in the correlated dynamics, the width for the center of mass, related to Re $A_{cm} = \sum_{ij}$ Re A_{ij}, behaves like the width of the Gaussian wave-packet for a particle with twice the nucleon mass. While the element A_{cm} decreases with time, it does so because the off-diagonal element A_{12} of the matrix increases in magnitude. The element A_{rel}, cf. below (6), stays constant.

As we have already demonstrated, for the uncorrelated dynamics an unphysical exchange of energy occurs between the internal degrees of freedom and the center of mass motion. When the magnitude of the internal energy exceeds the energy of localization of the center of mass, the coupling may cause unphysical oscillations for the ground state. This is shown for the α particle in Fig. 2. In the case of a correlated wave function, the width for the center of mass behaves as the width of a Gaussian packet for a particle with four times the nucleon mass. The internal part of the wave function does not change with time. In the case of an uncorrelated wave function initialized in the lowest state of internal energy, the matrix element and, correspondingly, the width for the center of mass oscillate. An exchange of energy, back and forth, occurs between the internal and center-of-mass degrees of freedom. If the uncorrelated wave function is initialized in the lowest state of total energy, the internal and center-of-mass energies stay constant. The internal wave function does not vary with time, but nor does vary the center-of-mass wave-function, with the center of mass never getting delocalized. Needless to say that in that case the internal energy is higher than in the ground state. The examples in Figs. 1 and 2 show the benefits of using the correlated over the uncorrelated wave functions in the fragment description.

Turning now to fragment production, we start out by exploring the situation where a highly excited system formed in the central heavy-ion collisions decays into vacuum. For such a system we expect a reduced importance of the antisymmetrization that is missing from our equations. We assume that internal degrees of freedom of the system are, generally, equilibrated, allowing only for a variable strength of the radial flow. We investigate the dynamics with a variable width matrix, either restricted or not to the diagonal form and, further, the dynamics with a static width, i.e. classical. More significant and surprising differences are found between the quantal and classical dynamics than between the dynamics with different variable width matrices.

To simulate the excited system ($A = 20 - 80$), we distribute centroids randomly within a spatial volume of radius R and in the momentum according to a finite-temperature Fermi distribution ($T = 5 - 12$ MeV). To account for the flow, we add to the momentum of each particle a component proportional to the position vector relative to the overall center of mass. The proportionality constant determines the amount of flow energy in the initial state ($E_{col} = 0 - 25$ MeV/nucleon). The width matrix is initialized as a real multiple of the unit matrix. Spatial representation of one of such initial states is given in Fig. 3a. In the particular case $A = 80$ and $R \simeq 5$ fm. The rms radii of individual packets are equal to 1.9 fm.

In the case of a dynamic matrix, whether or not restricted to a diagonal form, the excited system, initialized as above, emits a number of single nucleons in the course of time. The number of emitted nucleons generally increases with the energy of the system. However, at no particular energy, for the studied $A = 20 - 80$ systems, *any emission of IMF or even of α particles is observed.* This appears to be true irrespective of how we divide the excitation energy into collective and thermal. Examples of the late-stage distributions of centroids in space are given in Figs. 3(c) and 3(d) for the initial net excitation energy of 14 and 26 MeV/nucleon, respectively. For the particular initial states, the centroid distributions at the respective time are not distinguishable by eye between the evolutions with and without correlations. We found that frequently to be the case for the systems initialized in the manner discussed above. While some centroids appear close to each other in Figs. 3(c)

and 3(d), at a distance from the main residue, the respective wave-packet widths are so large that the packets will separate from each other, eventually. At $t = 300$ fm/c, for the displayed systems, all relative energies of the emitted particles are positive.

To check whether the lack of fragment production in the correlated dynamics might be associated with the initialization of the dynamics in an uncorrelated state, we have carried out tests using different initializations. Thus, we have added to the hamiltonian an oscillator term $V = v_{osc} \sum_i x_i^2$, to keep an excited system from expanding into vacuum, while allowing the matrix elements of A to thermalize, eventually removing this additional potential. Figure 4 shows the late stage of an $A = 80$ system initialized using a narrow oscillator potential. During the time of 100 fm/c within the oscillator potential, the rms values of off-diagonal elements of the matrix A had saturated, $\langle (\mathrm{Re}\, A_{i \neq j})^2 \rangle^{1/2} \sim 0.7/(A-1)$; for the chosen v_{osc} the system hardly expanded in the potential, compared to $t = 0$. On removing the constraining oscillator potential, we added collective components to particle momenta, proportional to the distance from the center. The system, subsequently, emitted a number of *single* nucleons and a deexcited residue formed at the center, consisting of 37 nucleons at the time shown in Fig. 4. In tests we changed the extension of the constraining oscillator potential for the excited nucleus, the initial temperature, and the magnitude of collective energy. Further, we initialized excited nuclei without any initial constraining potential, just assigning random gaussian values to the off-diagonal and diagonal elements of A, using the thermalized values from the oscillator potential as a guidance. Consistently, in all tests, the released nuclei emitted, in the course of their evolution, a number of single nuclei but never any IMF or even an α particle. Thus, the particular feature does not depend on the off-diagonal terms of A being zero or finite in the initial state of an excited nucleus.

Clearly, in the past, the production of IMFs and light clusters has been observed in the QMD calculations. The QMD limit corresponds to taking $\hbar \to 0$, or to suppressing the width dynamics in our equations. Indeed, when taking $\hbar$ reduced by a factor of (5–10), or the width dynamics slowed down by a such a factor, we begin to observe the cluster production. Figure 3(b) shows centroids for a system evolved from the initial state shown

in Fig. 3(a), using a static width, for the same available energy (given the frozen width) as the system in Fig. 3(c). At a time $t = 300$ fm/c in Fig. 3(b), two IMFs as well as two dinucleons are seen and they will remain stable. Additional small clusters have been emitted before $t = 300$ fm/c and left the displayed spatial region. As the reason for the lack of cluster production in the calculations with a dynamic width matrix (whether diagonal or not) emerges, in our tests, the spreading of wave functions towards the emission time. After packets get delocalized, the interaction is not capable to contract them back into fragments.

Our results on the cluster production for the dynamic width matrix may seem in contradiction to the FMD results [9] with even multifragmentation events reported in nuclear collisions. However, a scrupulous examination indicates that the clusters, seen in the final states of the FMD calculations in [9], were not formed during reactions, but were present in the initial states and survived reactions. When investigating that particular issue, we simulated symmetric collisions of nuclei with different initial structures. Thus e.g. for the potential (15) and our Pauli potential, the centroids within the ground state of ^{12}C form three α-type clusters of four nucleons each. On the other hand, within ^{40}Ca the nucleon centroids situate themselves at the overall center of mass position; the widths for different nucleons take on different values. In the true ground state for our potential, the momenta form groups of four in ^{40}Ca, with the four particles being two protons and two neutrons with different spin directions. To illustrate, though, our point on reactions, we shall displace slightly the momenta from the identical values in ^{40}Ca in the initial state of a reaction, making sure that change in the overall binding energy is negligible. Notably, inclusion of any kind of spin-isospin dependent interaction would break the momentum sub-clusters in nuclei of $A \leq 40$, anyway. Then, when considering the $^{12}C + ^{12}C$ reaction, we shall deal with six sub-clusters in initial state, and with none in the $^{40}Ca + ^{40}Ca$ case.

Figure 5 shows the initial and late states of an exemplary $^{12}C + ^{12}C$ reaction at the beam energy of 29 MeV/nucleon. While one nucleus got highly excited in the reaction, the other has fragmented into three α particles. Each of the α particles is excited at the displayed time, however remaining below threshold for particle emission.

Figure 6 shows three stages of a 35 MeV/nucleon $^{40}Ca + ^{40}Ca$ reaction with no subclusters in the initial state. At the first of the times shown, the wave functions of the two nuclei just started to overlap. At the second of the times, a transient residue that formed is maximally spread out. At the third of the times, the outcome of the collision is, essentially, determined and only a residue and some single nucleons are seen. No clusters are emitted from this collision.

The examples presented in Figs. 5 and 6 are typical ones: for none of the studied initial states, we have observed, for the dynamic width, the emission of IMF's or of α particles that were not present in the substructure of an initial state. This has been the case whether we included or excluded the correlations. Again, as a reason for the absence of cluster formation for the dynamic width, we find that, at times when the system reaches a density when clusters are expected to form, the width of the wave packets has grown so large that the interaction between different wave packets is too weak to force the width of these packets to shrink, and their centroids to approach each other enough to form a nucleus (see also [18]). When we suppress the dynamics of the matrix A, new clusters form and emerge from the reaction region.

The values of the widths are not necessarily unphysically large, as nucleons are expected to get delocalized with the reaction progress. In reality, though, when broad wave packets of different nucleons overlap in space, the interaction between the nucleons should be generally able to clump two or more nucleons, within a distance comparable to the interaction range, into a cluster. The wave function in terms of broadened Gaussians (whether or not diagonal in the nucleon coordinates) does not allow for that.

VI. SUMMARY AND CONCLUSIONS

We have investigated the time evolution of nuclear systems, in terms of correlated and uncorrelated Gaussian wave functions, following from the time variational principle. As an interaction in the Hamiltonian, we utilized a Volkov-type potential. Upon determining that

an antisymmetrization of the correlated wave function would not be feasible beyond relatively small systems, we employed a Pauli type potential to simulate the effects of Pauli principle.

For uncorrelated trial wave functions, the internal state cannot be localized without localizing the center of mass. Thermal estimates indicate that this could suppress fragment emission. In dynamics, an unphysical energy exchange occurs between the center of mass and the intrinsic motions. These deficiencies are absent when using the *correlated* wave functions. We have explicitly demonstrated an improvement, in terms of correlated wave functions, in the description of deuterons and alphas.

Contrary to expectations, the inclusion of correlations has not improved the description of cluster production in the explicit simulations of heavy-ion reactions or in situations characteristic for the reactions. Either in correlated or uncorrelated Gaussian dynamics, clusters are *only* produced when they are present in the substructure of an initial state. This appears to be true, in the correlated dynamics, whether or not the initial state is correlated. The absence of new clusters is associated with a large spreading of the wave function at the time when a reacting system expands and the new clusters are expected to form. The spreading in relative coordinates is present even in the correlated wave function, despite of the fact that, for a correlated wave function, the relative spreading may evolve independently from the spreading for the center of mass for any of the potential fragments. The interaction is too weak to pull back the wave function to a size appropriate for a fragment. In classical dynamics fragments are produced.

While there is nothing unphysical in the spreading of the wave function as such in the simulations, in reality the interaction would be capable of creating correlations in the wave function over distances of the interaction range. E.g., when considering the two-nucleon correlation function, with time the function should develop into a spreading long-range component, weighted with a certain probability, and a more stable short-range component corresponding to the forming fragments. The specific parametrization of the wave function, once the wave function has spread, does not allow for the development of the short-range

component.

On a general level our results show that the dynamics is important in fragment production. The spread of the wave packets at emission indicates that an emitting system can gain the packet delocalization energy. On the side, within AMD the width dynamics is suppressed and an *ad hoc* term is added to the Hamiltonian to account for the delocalization at emission. Within QMD, the location energy is disregarded at every stage, including the initial ground-state nuclei and the final state. Practically, the procedure in AMD amounts to a change in the effective interaction, compared to QMD. Within either the approaches, the fixed width of a wave packet extends the range of the two-particle interaction and may, in fact, act to suppress fragment formation.

Recent results from FMD with short-range correlations [19] show some fragments in the final state of reactions, in contrast to the present calculations (or [18]). This can be attributed to a lesser spreading of the wave packets towards emission time, due to the combination of the effects of short-range correlations and the assumed spherical shape of packets. Given that this lesser spreading is unrelated to the physics of fragment production, we believe that it is not a solution to the the dilemma at hand. In particular, we expect too low fragment yields, from the calculations with short-range correlations, compared to experiment.

We conclude that, in a successful description of fragment production, the wave function or, more generally, the model density matrix must a have a flexibility to change over distances comparable to the interaction range, at a time when the fragments are formed. One possibility within the dynamics is to keep the nucleon wave-packet width static and comparable to the interaction range, and to account for a quantal spreading with time through a stochastic decision process [20]. This can be nominally derived through the reduction of the wave function space to the space spanned by the wave packets of constant width, which results in a residual force associated with the kinetic-energy part of the hamiltonian. The present authors have been exploring a replacing of the single wave packet for every nucleon by a superposition of packets. Unfortunately, this looses the inherent simplicity of FMD. The high hopes associated with the FMD approach cannot be directly realized as

far as fragmentation is concerned.

ACKNOWLEDGMENTS

The authors benefited from discussions with H. Feldmeier, J. Schnack, and M. Płoszajczak. Suggestion of H. Feldmeier to investigate an initial state with long-range correlations is appreciated. This work was partially supported by the Deutsche Forschungsgemeinschaft and by the National Science Foundation under Grant No. PHY-9403666.

REFERENCES

[1] Proc. XXII Workshop on Gross Properties of Nuclei and Nuclear Excitations, Hirschegg, 1994, ed. H. Feldmeier (Gesellschaft für Schwerionenforschung, Darmstadt, 1994).

[2] G. F. Bertsch and S. Das Gupta, Phys. Reports 160 (1988) 189.

[3] S. Ayik and C. Gregoire, Nucl. Phys. A513 (1990) 187.

[4] J. Randrup and B. Remaud, Nucl. Phys. A514 (1990) 339.

[5] M. B. Tsang, private communication, November 1994.

[6] J. P. Bondorf et al., Phys. Lett. 162B (1985) 30.

[7] D. H. E. Gross, X. Z. Zhang, and S. Y. Xu, Phys. Rev. Lett. 56 (1986) 1544.

[8] H. Feldmeier, Nucl. Phys. A515 (1990) 147.

[9] H. Feldmeier, K. Bieler and J. Schnack, Nucl. Phys. A586 (1995) 493.

[10] A. Ono, H. Horiuchi, T. Maruyama and A. Ohnishi, Phys. Rev. Lett. 68 (1992) 2898.

[11] T. Maruyama, K. Niita and A. Iwamoto, Phys. Rev. C53 (1996) 297.

[12] J. Aichelin and H. Stöcker, Phys. Lett. B176 (1986) 14.

[13] T. Maruyama, A. Ohnishi, and H. Horiuchi, Phys. Rev. C42 (1990) 386.

[14] A. Bohnet et al., Phys. Rev. C44 (1991) 2111.

[15] P. B. Gossiaux, D. Keane, S. Wang, and J. Aichelin, Phys. Rev. C51 (1995) 3357.

[16] D. M. Brink and E. Boecker, Nucl. Phys. A91 (1967) 1.

[17] A. B. Volkov, Nucl. Phys. A74 (1965) 33.

[18] Ph. Chomaz, M. Colonna, and A. Guarnera, Proc. 12th Winter Workshop on Nuclear Dynamics, Snowbird, 1996, ed. W. Bauer (Plenum, New York, 1996) p. 65.

[19] H. Feldmeier and J. Schnack, private communication, June 1996.

[20] A. Ohnishi and J. Randrup, Phys. Rev. Lett. 75 (1995) 596.

FIGURES

FIG. 1. Evolution for the internal ground state of a free deuteron. (a) The dashed, solid, dash-dotted, and dotted lines show, respectively, the evolution of the kinetic, total, internal, and potential energies in correlated (c) and and uncorrelated (u) dynamics. (b) Evolution of the elements of the width matrix. The dashed lines shows the evolution of the element in the case of an uncorrelated wave function. The dash-dotted, solid, and dotted lines show, respectively, the evolution of the internal, center-of-mass, and diagonal elements in the case of a correlated wave function, cf. Eq. (6) and text below.

FIG. 2. Evolution of the elements of the width matrix A for an α particle initialized in its ground state. The solid, dash-dotted, and dotted lines show, respectively, the evolution of the center-of-mass, relative between-two-nucleons, and diagonal elements, in the case of a correlated wave function, cf. Eqs. (6) and (2). The long-dashed line shows the evolution of the element in the case of an uncorrelated wave function initialized in the lowest state of internal energy. The short-dashed line shows the evolution of the element in the case of an uncorrelated function initialized in the lowest state of total energy.

FIG. 3. Particle centroids (dots) in the configuration space for $A = 80$, in the initial state (a) and at $t = 200$ fm/c for the static wave-packet width (b), and for the dynamic width matrix (c) and (d). In (c), the initial flow energy is lowered, compared to (b) and (d), by the initial energy content in the localization of the wave packets. The circles indicate rms radii of the most and least localized Gaussians. The radii of the packets in the case (b), and the radii of the most localized packets in the case (c), are comparable to the radii of the dots representing centroids. The axes show distances in fm.

FIG. 4. Late stage (t = 300 fm/c) of an $A = 80$ system initialized at a temperature $T = 8$ MeV and $E_{col} = 0$ in a narrow oscillator potential $V = v_{osc} \sum_i x_i^2$, where $v_{osc} = 1$ MeV/fm^2. At a time $t = 100$ fm/c, the oscillator potential was removed, and particles given collective outward velocities corresponding to net $E_{col} = 7$ MeV/nucleon. The centroids for emitted and bound particles (negative and positive removal energies, respectively) are indicated with small open and small filled circles, respectively. The large circles indicate widths, from the diagonal elements of A, for most localized and delocalized bound and emitted particles.

FIG. 5. Initial (left side) and late (t = 300 fm; right side) states of a $^{12}C + ^{12}C$ reaction at 29 MeV/nucleon. The beam axis is directed vertically, dots represent the centroids of nucleon packets, and circles show the packet rms radii. Edges of the spatial boxes show distances along the carthesian axes in fm.

FIG. 6. Three stages of a 35 MeV/nucleon $^{40}Ca + ^{40}Ca$ reaction in the configuration space. From left to right, the boxes show the reaction, respectively, at $t = 20$ fm/c, $t = 100$ fm/c, and $t = 300$ fm/c. The dots indicate centroids, while the circles indicate the rms radii of the least and most localized Gaussians. Box edges show the distances along the carthesian axes in fm.

figure 1

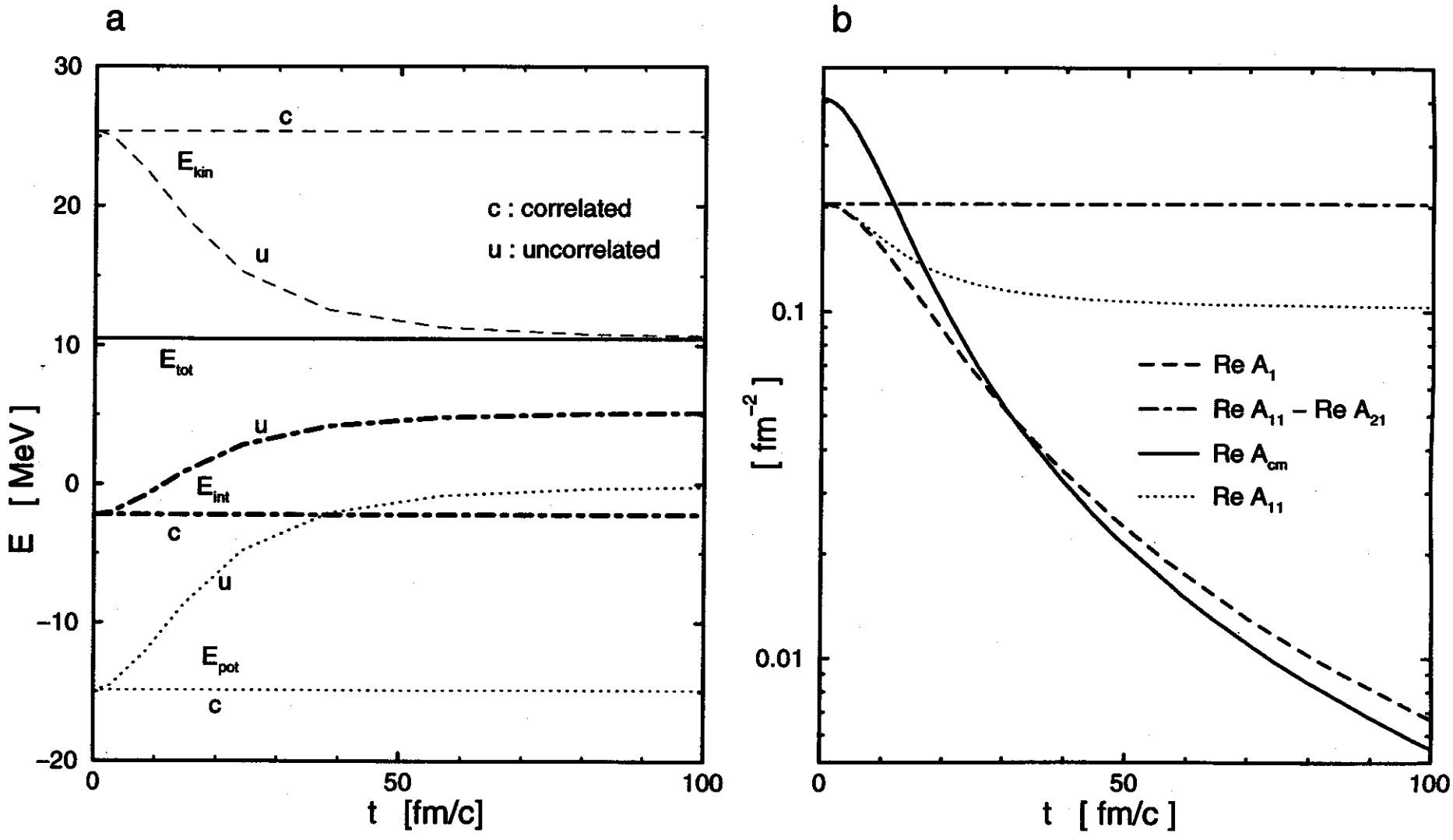
a
b
30
20
10
0
−10
−20
E [MeV]
c
E_kin
u
c : correlated
u : uncorrelated
E_tot
u
E_int
c
u
E_pot
c
0
50
100
t [fm/c]
0.1
0.01
[fm^-2]
Re A_1
Re A_11 − Re A_21
Re A_cm
Re A_11
0
50
100
t [fm/c]

figure 2

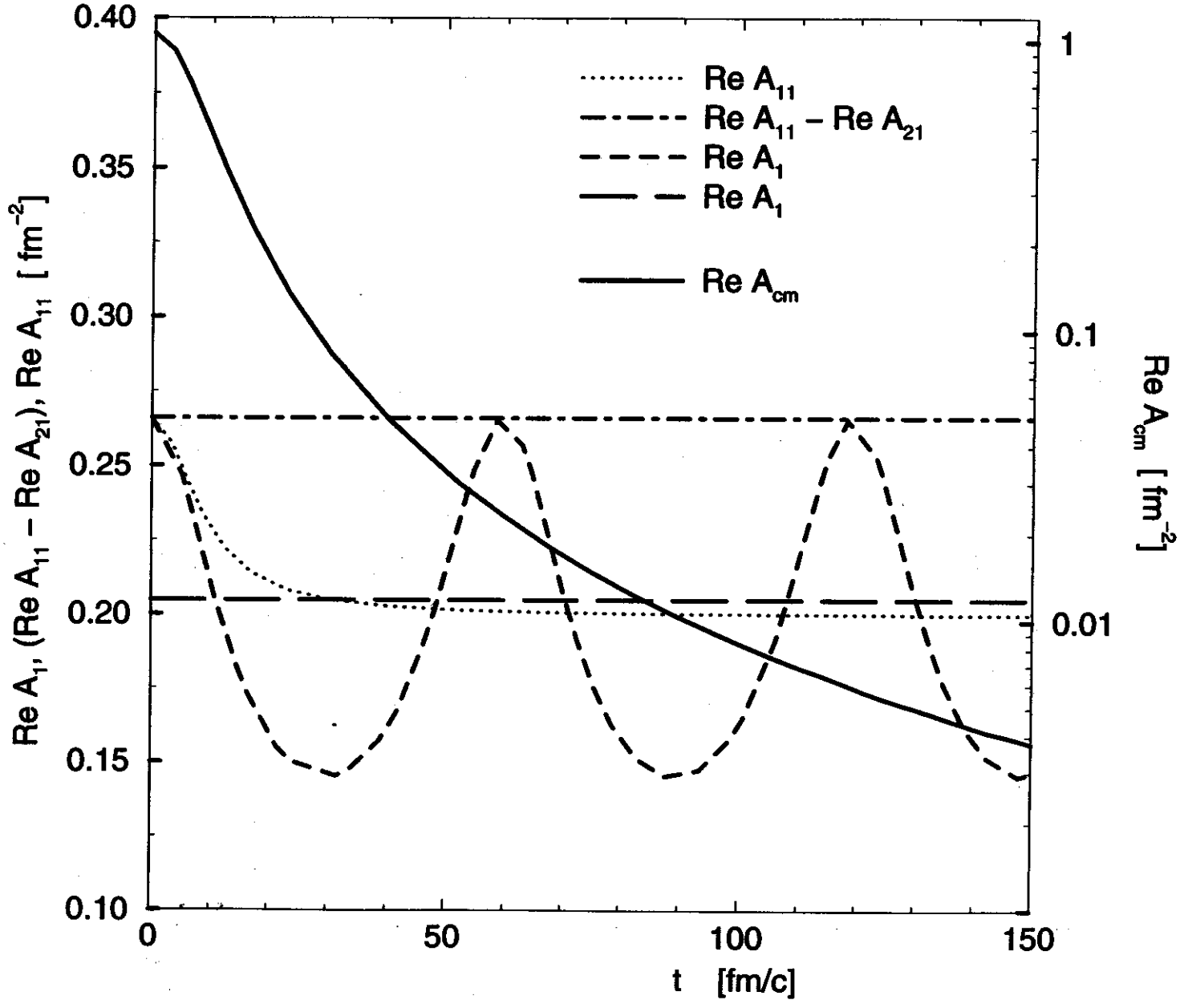
0.40
0.35
0.30
0.25
0.20
0.15
0.10
0
50
100
150
t [fm/c]
1
0.1
0.01
Re A11
Re A11 – Re A21
Re A1
Re A1
Re Acm
Re A1, (Re A11 – Re A21), Re A11 [fm-2]
Re Acm [fm-2]

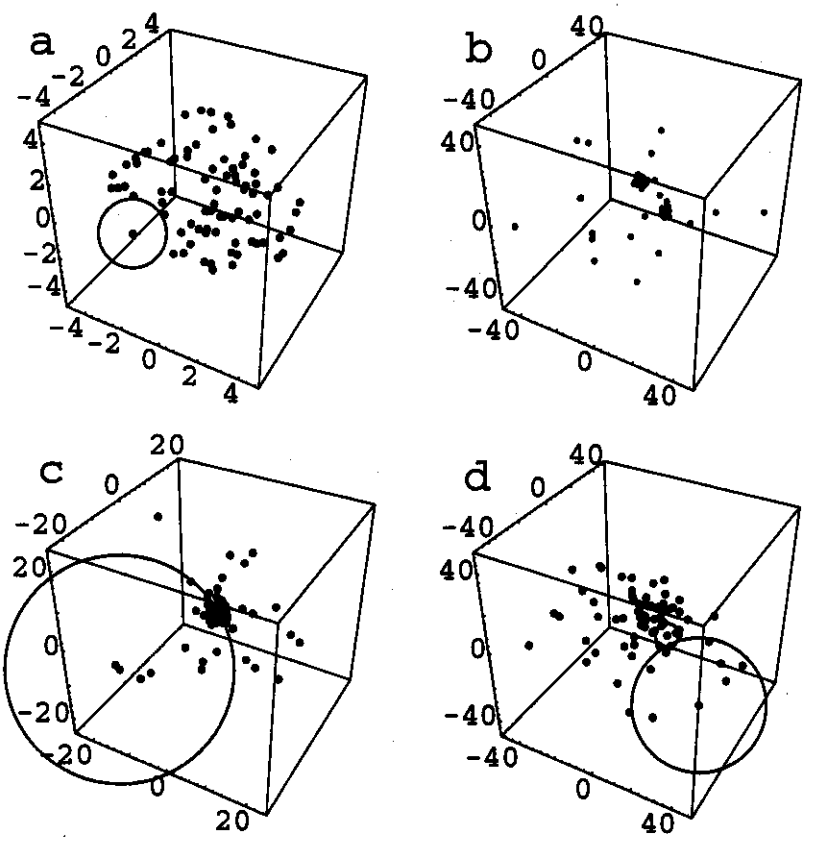
a
4
2
0
-2
-4
4
2
0
-2
-4
-4 -2 0 2 4
b
40
0
-40
40
0
-40
-40 0 40
c
20
0
-20
20
0
-20
-20 0 20
d
40
0
-40
40
0
-40
-40 0 40

figure 3

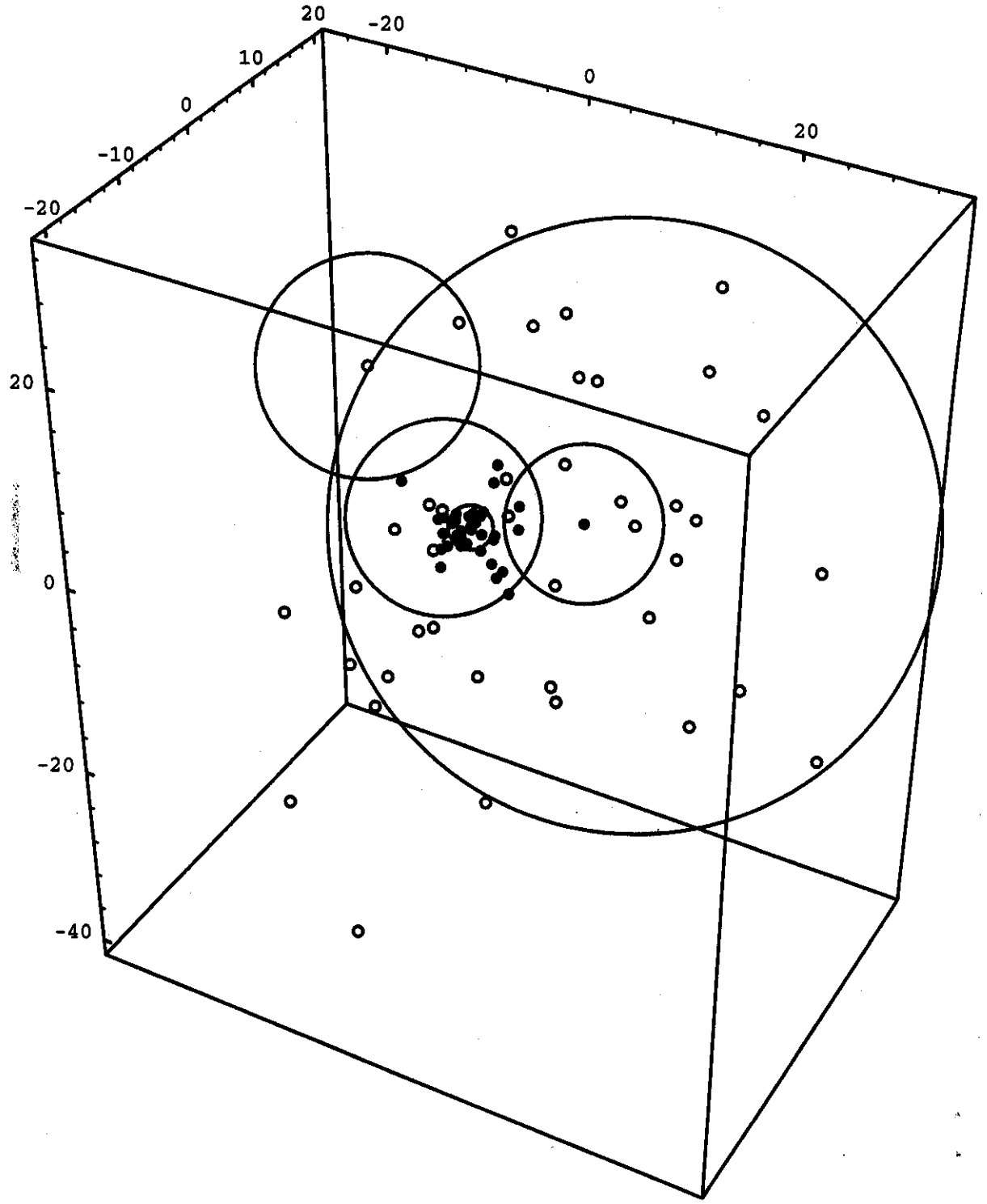

figure 4

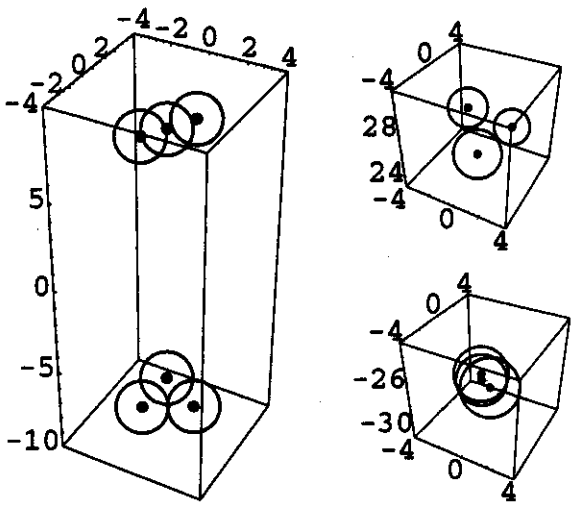

figure 5

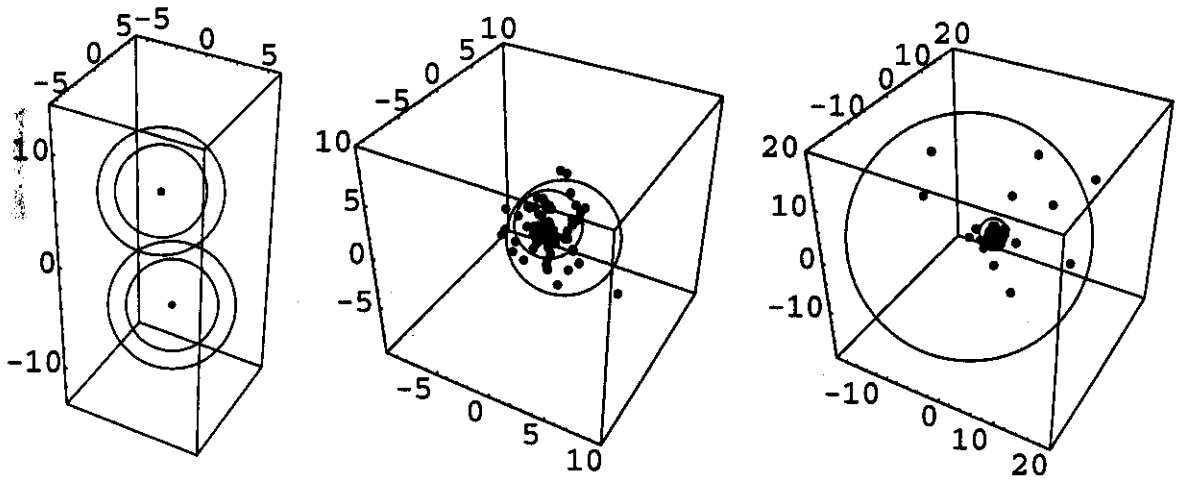
5 -5 0 5
-5
10
0
-10
10 5 10
-5 0 5
10
5
0
-5
-5 0 5 10
20 10 20
-10 0 10
20
10
0
-10
-10 0 10 20

figure 6